REPORT DOCUMENTATION PAGE

AFRL-SR-AR-TR-06-0346

1. REPORT DATE *(DD-MM-YYYY)*	2. REPORT TYPE	3. DATES COVERED *(From - To)*
31 07 2006	FINAL REPORT	1 MAY 01 TO 30 APR 06

4. TITLE AND SUBTITLE

IN SITU EXPERIMENTAL STUDIES OF FUNDAMENTAL DEGRADATION PROCESSES IN THE LOW EARTH ORBIT INVIRONMENT

5a. CONTRACT NUMBER

5b. GRANT NUMBER
F49620-01-1-0336

5c. PROGRAM ELEMENT NUMBER
61103F

6. AUTHOR(S)
DR JUDITH C.YANG

5d. PROJECT NUMBER
5094

5e. TASK NUMBER
RS

5f. WORK UNIT NUMBER

7. PERFORMING ORGANIZATION NAME(S) AND ADDRESS(ES)
UNIVERSITY OF PITTSBURGH
MATERIALS SCIENCE AND ENGINEERING DEPARTMENT
848 BENEDUM HALL, PITTSBURGH, PA 15213

8. PERFORMING ORGANIZATION REPORT NUMBER

9. SPONSORING/MONITORING AGENCY NAME(S) AND ADDRESS(ES)
AFOSR/NL
875 NORTH RANDOLPH STREET
SUITE 325, ROOM 3112
ARLINGTON, VA 22203-1768
Maj Jennifer Gresham

10. SPONSOR/MONITOR'S ACRONYM(S)

11. SPONSOR/MONITOR'S REPORT NUMBER(S)

12. DISTRIBUTION/AVAILABILITY STATEMENT
APPROVE FOR PUBLIC RELEASE, DISTRIBUTION UNLIMITED

13. SUPPLEMENTARY NOTES

14. ABSTRACT
The primary accomplishment of this MURI team was demonstrating that completed different oxides form due to exposure to hyperthermal atomic oxygen, and, hence, novel oxidation mechanisms are needed to explain such unusual oxide structures. ITO: the reactivity of AO causes recrystallization of the ITO nanograins along the interface between the ITO and substrate, which would negatively affect the film adhesion. Si: Remarkably homogeneous and uniform oxides form that are thicker and more ordered towards the alpha quartz structure than the oxide formed by O2 exposure, due to the high reactivity of the AO and its kinetic energy. Ge: The effect of the AO is to produce smaller nanograins of crystalline GeO2 as compared to O2, where increasing the kinetic energy increases the oxide thickness. Al: The AO causes initial vaporization and corresponding roughening of the Al surface prior to the growth of the amorphous oxide scale, which could be due to the information of gaseous and stable AlO2.

15. SUBJECT TERMS

16. SECURITY CLASSIFICATION OF:			17. LIMITATION OF ABSTRACT	18. NUMBER OF PAGES	19a. NAME OF RESPONSIBLE PERSON
a. REPORT	b. ABSTRACT	c. THIS PAGE			
					19b. TELEPHONE NUMBER *(Include area code)*

Standard Form 298 (Rev. 8/98)
Prescribed by ANSI Std. Z39.18

IN SITU EXPERIMENTAL STUDIES OF FUNDAMENTAL DEGRADATION PROCESSES IN THE LOW EARTH ORBIT ENVIRONMENT

FINAL REPORT
August 1, 2006

Principal Investigator: Judith C. Yang, University of Pittsburgh

Address: Materials Science and Engineering Department
                        848 Benedum Hall
                        University of Pittsburgh
                        Pittsburgh, PA 15213
                        Jyang@engr.pitt.edu

Co-Principal Investigators: John T. Yates, Jr.
                               Chemistry Department
                               University of Pittsburgh

                               Ian Robinson
                               Physics Department
                               University of Illinois at Urbana-Champaign

                               Robert Averback
                               Materials Science and Engineering Department
                               University of Illinois at Urbana-Champaign

                               George Schatz
                               Chemistry Department
                               Northwestern University

                               Paul Voyles
                               Materials Science and Engineering Department
                               University of Wisconsin at Madison

A. OBJECTIVES

The objective of this MURI program was to gain fundamental and predictive understanding of the primary degradation mechanisms experienced by low Earth orbit (LEO) vehicles. Space vehicles to be employed in LEO will be subject to harsh environments that can greatly hasten their failure. Since primary damage results from collisions with atomic oxygen (AO), we focused our efforts on the effects of hyperthermal atomic oxygen on the structure of model systems. Since secondary effects, such as charging, also exist in LEO, we also investigated the synergistic effects of charging on oxidation.

To gain fundamental insights into the fundamental surface passivation mechanisms of metal and semiconductor materials in LEO environment by using complementary experimental techniques, including surface science methods (John Yates, UPitt), synchrotron X-ray diffraction (XRD) (Ian Robinson and Robert Averback, UIUC) and advanced transmission electron microscopy (TEM) (Judith Yang, UPitt; Paul Voyles, UWisc.), as well as modeling (George Schatz, Northwestern). Each group focused on the same model metals (Al and Ag) and semiconductors (Si, Ge, ITO). These model materials were selected for their applications in LEO, esp. as coating materials for polymers that rapidly erode in this harsh environment. Also, metals are often used as structural components in space vehicles and semiconductors are used for devices as well as solar cells in LEO.

Our major discovery is that for all materials systems studied, hyperthermal atomic oxygen gave quite remarkably different oxide structures and, hence fundamentally and completely different oxidation mechanisms must be occurring than that by molecular oxygen. In particular, novel oxidation models have been developed to explain the structural changes observed for Ag, Al and Si oxidation.

B. PERSONEL

The program started on May 1, 2001, with originally Judith Yang (UPitt), John T. Yates, Jr. (UPitt), Ian Robinson (UIUC) and Robert Averback (UIUC). In the final year Yates, due to his pending retirement, withdrew from the MURI program, and Paul Voyles (Wisc.) and George Schatz (Northwestern) joined the MURI program.

Post-docs and research associates: Long Li (UPitt), Shenya Ohno (UPitt), Sanjit Ghose (UIUC), Ross Harder (UIUC), Christine Aikens (Northwestern)

Graduate Students: Maja Kisa (UPitt), William Stratton (Wisc.), Irene Popova (UPitt), Zhi Chen (UPitt), Joshua Middendorf (Northwestern).

C. ACCOMPLISHMENTS:

C.1.a. Development of Lab-based Instrumentation to Best Mimic LEO

The critical aspect of this program was the oxygen source that will best mimic the hyperthermal (5eV) atomic oxygen in the low Earth orbit. We originally designed and built an O_2^+ gun as a low cost source in the first year of this program. Fortunately, in 2002, we received a DURIP grant for the purchase of a Physical Sciences Inc (PSI) hyperthermal atomic oxygen source based on the laser detonation of O_2 gas, that best mimics the atomic oxygen in LEO.

C.1.a.i. Development of Low-Cost O_2^+ Ion Gun to Produce Hyperthermal Atomic Oxygen on Metals and Semiconductor Surfaces

The first low-cost source was based on the highly efficient neutralization of accelerated O_2^+ ions when they approach a metal or semiconductor surface. The O_2^+ source was optimized to deliver a large fluence to a surface to produce atomic oxygen species with average of 5 eV kinetic energy. When the incident O_2^+ ions carry a certain kinetic energy and when they are rapidly neutralized, the excess kinetic energy is partitioned between the two O atoms that are dissociating at the surface. The essential features included operating the gun at initial ion energies for which the guns was designed up to +5KeV for positive ions. By floating the outer case of the gun at high negative potentials, low ion energies were produced. The energy generated in the original power supply minus a retarding potential that was applied at the sample equals the energy of the ions incident on the sample (figure 1). In the modified ion gun, most of the electrostatic retardation occurs near the exit region of the gun. The beam size and energy spread as a function of the electrode potential was tested for Ar^+ ions on Al. The beam size was defocused by 15-30 % as compared to the normal mode operation. The beam energy was adjustable in 10-5000±1 eV range with ion currents up to 5 $\mu A/cm^2$. But, the energy spread of the beam was measured to be ~10eV FWHM for V_{ps} = 30V. However, since the spacecraft surface is rough, then the atomic oxygen strike the surface with various angles of incidence, thereby giving a range of normal kinetic energies to the surface around 5eV. Hence, the range of energies of AO from this O_2^+ ion gun source is similar to the range of energies of AO incident upon a spacecraft.
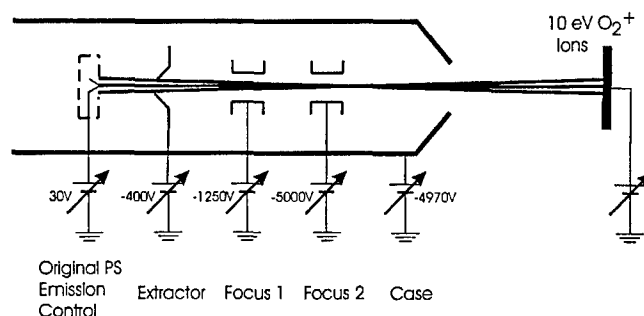

Figure 1. Schematic diagram of the Ion Gun used to produce low energy O_2^+.

C.1.a.ii. Pitt PSI FAST AO Source

In 2002, we received a DURIP grant (350K) to purchase a hyperthermal atomic oxygen source from Physical Sciences, Inc (PSI). Bob Krech from PSI installed this machine at Pittsburgh in October 2004. During the installation of this source, we collaborated with Tim Minton, who has a similar source, for *ex situ* exposures of Ag, Al, and Si samples by 5 eV AO. Several modifications were made to this Pitt PSI FAST AO source for ultra-high vacuum (6×10^{-9} torr), internal bake-out system, dual-head quartz crystal microbalance (QCM), a heating stage (up to 2000K), and this year a VUV (vacuum ultraviolet) lamp (figure 2). The combined abilities of VUV, heating and tunable energy eV (4-15 eV) high flux atomic oxygen provides a unique lab-based source that best mimics the conditions in the LEO. As part of the MISSE-6 mission, we will directly compare identical metal and semiconductor samples that are exposed in LEO to those exposed in our AO source to quantify how well and to what length-scale, this ground based source simulates the LEO environment.

3

The dual sensor head QCM system permits the dynamical measurements of mass changes of two films simultaneously during AO exposure with extremely high mass-resolution of 0.4 ng/cm^2 (frequency resolution of 0.03 Hz at 6 MHz) and high stability ($\Delta m < 10$ $ng/cm^2/hour$). Recently the top flange where the conical nozzle is placed, has been modified to include 6 specially designed ports (inclined at various angles and lengths) for future sources or detectors. On one of these ports, we attached a newly purchased VUV lamp in order to expose samples at different positions including the QCM samples.
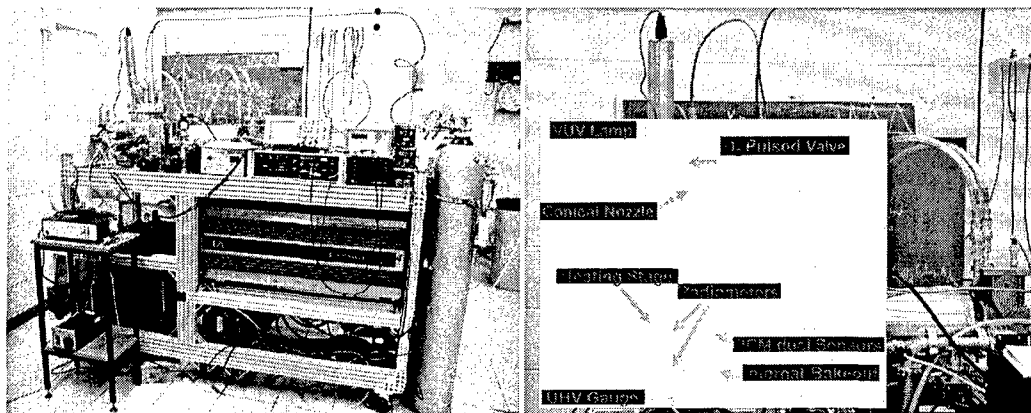

Figure 2. The Pitt FAST^{TM} AO source (left) and the close-up of the chamber(right) with VUV lamp. The base and working vacuum are about 6×10^{-9} and 2×10^{-8} torr, respectively.

The Resonance Ltd. is the best VUV lamp supplier for LEO simulation. The Resonance RF-powered D2ArCM-C deuterium lamp is a low-pressure lamp that supplies VUV radiation with a sharp spectrum at 121.6 nm, corresponding to the hydrogen Lyman alpha line, with a solid angle of 26 degree. This lamp can well simulate the VUV in the LEO environment. With these additional modifications to the Pitt FAST AO source, it is the best overall ground-based source to mimic LEO in a controlled environment. Another unique feature of this source is its portability, such that it can be moved to advanced characterization sites, such as synchrotrons.

C.1.b. Effects of Hyperthermal Atomic Oxygen on Semiconductors

C.1.b.i. Interfacial Crystallization of ITO by Reactive Atomic Oxygen Exposure of ITO Thin Films

Indium tin oxide, ITO, is a compound oxide known as semi-metal or n-type semi-conductor with precious properties, such as high optical transparency mostly to visible light and electrical conductivity. The main application of ITO in LEO is used as a coating material for polymers, such as solar cell blankets that are made of Kapton or polyester. The ITO coating functions for i) AO-erosion protection, and ii) for bleeding off static charges on the insulated polymer surface which were primarily from the charge species in the LEO environment. The coated ITO/float glass with In_2O_3: 10w% SnO_2 possesses a complex BCC structure, so called cubic bixbyite structure, with a stoichiometric formula of $In_{2-x} Sn_x O_3$. The lattice parameter a = 1.0168 nm.

The ITO/SiO_2/float glass samples, with a thickness of around 200 nm (180-220 nm) and surface resistivity of 4-8 ohm were exposed to the hyperthermal AO source that resides at the University of Pittsburgh. Films with four separate exposures to 5eV AO (fluences of 0, 2×10^{19}, 6×10^{19} and 2×10^{20} atoms/cm^2) were compared with an identical unexposed film to determine the effect of the atomic oxygen.

4

Grazing incidence x-ray diffraction was chosen for its high degree of surface sensitivity as well as its ability to give depth profile information from within the film. These measurements were done at beamline 34_ID-C at the Advanced Photon Source (APS), Argonne National Lab. The high intensity of the APS allowed us to directly image the powder diffraction of the amorphous ITO film using a CCD (figure 3). Of the two powder rings access able to the detector the one at 2.5Å^{-1} was chosen for its relatively high intensity at an incidence angle slightly above the critical angle for the ITO/air interface. Many frames like those shown were collected while
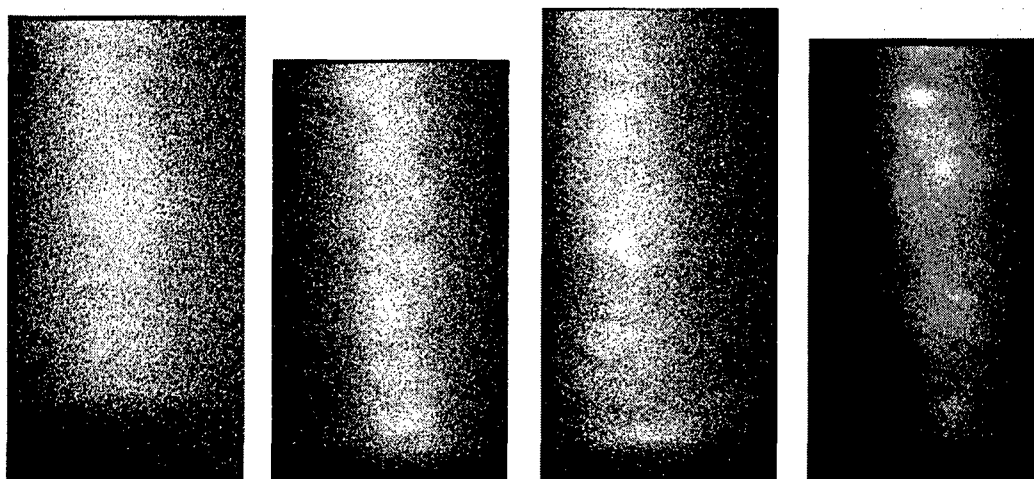

Figure 3: AO-induced crystallization of ITO thin films. Grazing incidence X-ray diffraction of the (400) ITO powder ring, measured at the Advanced Photon Source, Argonne, shows increasing crystallinity with dose. The crystallisation effects are strongest at the top of the diagrams where the diffraction comes from the interface and not just the surface region of the films.
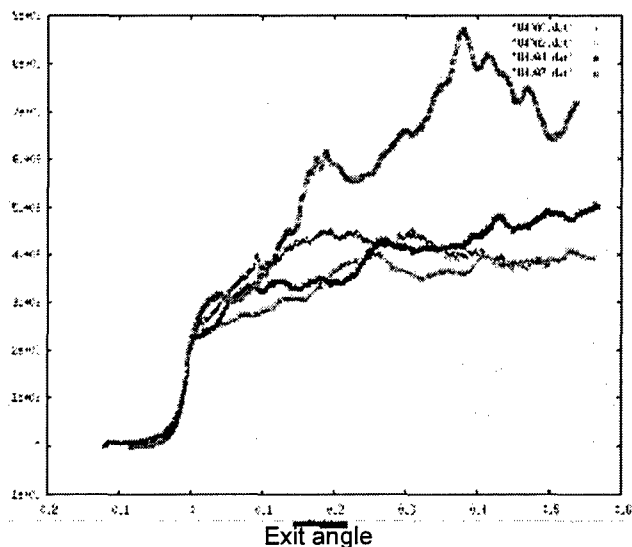

Figure 4. Integrated intensity profile as function of exit angle for increasing AO dose.

moving the sample within the beam. The frames were then added together and then integrated from left to right to condense the diffraction patterns into an intensity profile as a function of exit

angle for each sample. These intensity profiles illustrate the strong dependence of the crystallinity of the film on AO dose. The stronger Bragg reflections of larger crystallites give bright spots in the powder ring which then manifest themselves in the exit angle profiles as sharp peaks (figure 4).

The red curve shows the integrated intensity profile for the film that was not exposed to the AO source. It's relatively flat character for angles above the critical angle show that the film is fairly homogeneous in nature. The green and blue profiles show evidence of greater crystalline structure within the film. The most striking is the result for the most heavily dosed film, shown in purple. The sharp peaks illustrate a significant modification of the film by the AO. Also, the fact that the greatest peaks occur at the higher exit angles is evidence that the larger crystallites are localized deep within the film, near the interface. The interface localized preference for crystallization of ITO by AO could be a contributing factor to the delamination seen in low Earth orbit by these films.

The structural characterizations were carried out with scanning electron microscopy (SEM) and atomic force microscopy (AFM) for surface investigations and cross-sectional (S)TEM for ITO/substrate observation.
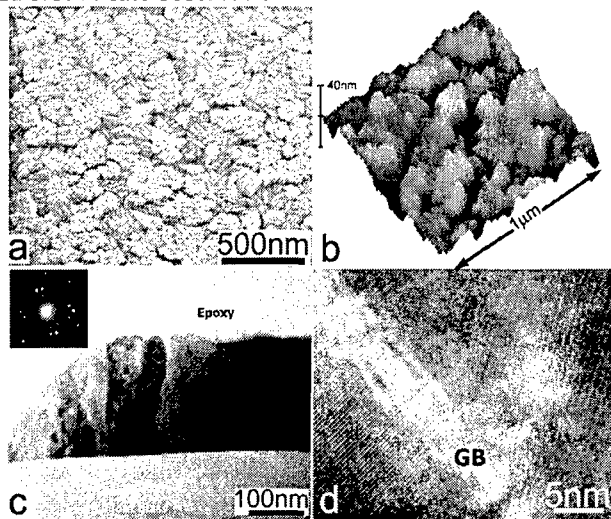

Figure 5. Structural information for the original ITO films before AO exposure.

Figure 5 is a set of images of structural information for the original ITO film before oxidation. Figure 5a is a SEM image which shows the ITO grains in bundles on the surface. The two kinds of grains, one with round shape with diameters ranging 20-50 nm and the other one with needle-like shape of 20-50 in width by ~100 nm in length. Figure 5b is AFM image showing the surface of original ITO film with a roughness of 5.3 nm of RMS. Figure 5c is a cross-sectional TEM image showing the structure of the ITO film and its substrate. The ITO film with a thickness of ~210 nm were grown on float glass with a ~50 nm intermediate amorphous SiO_2 as a passivated layer to prevent metallic ions, such Ca^{++} and Na^+ in float glass diffusing to ITO film. The interface of ITO/SiO_2 is clean and sharp. The ITO film is comprised with columnar grains with ~40 nm in width. Broad grain boundaries show between the columnar grains, seeing figure 6d, the HRTEM image of a typical grain boundary. Chemical analysis shows the ITO film composed with O, In and Sn., with a chemically abrupt ITO/SiO_2 interface.

We chose an ITO sample exposed with a fluence of 2×10^{20} atom/cm^2 to prepare cross-sectional TEM sample. Figure 6 is the results from cross-sectional TEM investigations. Many particles appeared in the SiO_2 substrate near interface, as compared with the clean interface of the unexposed ITO film. The particles are crystalline (figure 6b). By elemental analysis, these nanograins were identified as ITO particles in the SiO_2 substrate (figure 6d).
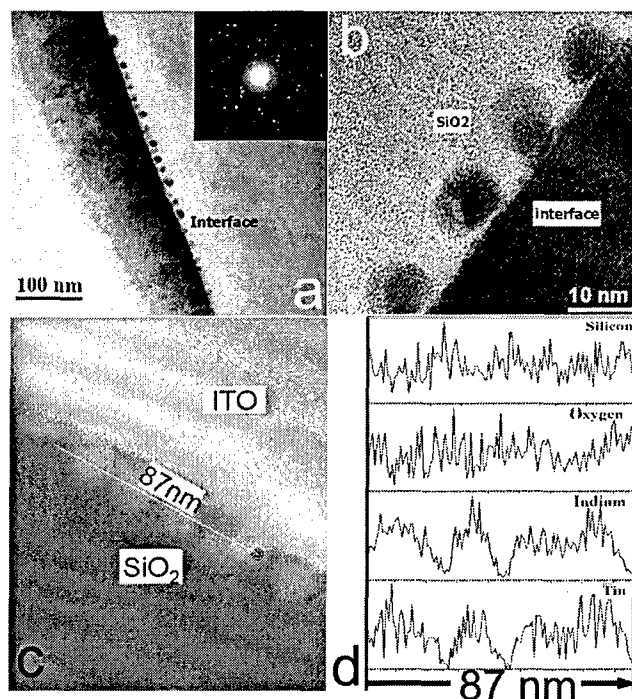
6

Figure 6. a. Cross-sectional TEM image of ITO film, HRTEM of the interface of ITO/SiO₂, and HAADF image as reference image for EDS line scan, which is shown in d, after exposed to AO, fluence of 2×10²⁰ atom/cm².

C.1.b.ii. Homogeneous Silica Formation on Si(100) by Hyperthermal Atomic Oxygen as compared to Molecular Oxygen

We investigated structural characteristics of a silica layer and Si/SiO_2 interface formed on Si(100)-single crystal by oxidation in hyperthermal atomic oxygen (AO) and molecular oxygen (MO). Several characterization techniques were used, and the data, as well as the models used to explain and understand obtained results are represented below.

Rutherford backscattering spectroscopy (RBS), synchrotron X-ray diffraction, advanced and cutting-edge electron microscopy techniques, such as high resolution transmission electron microscopy (HRTEM), electron energy loss spectroscopy (EELS). And fluctuation electron microscopy (FEM), and atomic force microscopy (AFM), were applied *ex situ* to 5 eV AO and MO formed oxides on Si(100). We observed that 5eV AO-exposed Si formed twice as thick oxide (5 nm compared to 3 nm), more homogeneous with a chemically abrupt interface 5nm thick oxide layer on Si(100) substrate, while the oxidation in MO produced only 3nm thick oxide scale. We examined the oxide thickness as a function of kinetic energy of the AO, and found increasing oxide thickness with increasing eV.

The Si/SiO_2 interface was found to be very smooth and abrupt for Si(100) oxidized by AO as compared to the rough interface formed by MO oxidation. The electron energy loss spectroscopy (EELS) line spectra revealed the nanoscale uniformity of the oxide formed by AO. Both $SiL_{2,3}$ and OK ionization edges from the EELS spectra revealed a chemically abrupt Si/SiO_2 interface for the Si(100) sample oxidized by AO (Figure 7), in contrast to the ~1 nm interfacial

7

transition layer when the oxide was grown in MO. Characteristic $SiL_{2,3}$ background subtracted edges obtained from Si(100) single crystal oxidized by AO are shown in Figures 7b, which show peaks corresponding to only Si^0 and Si^{4+} valence states, similar to what was previously determined by XPS . The abruptness in changing valence state from Si^0 to Si^{4+} at the interface was always observed for the AO-oxidized sample, while for the MO-oxidized sample, no chemically abrupt transition in oxidation state was noted at the Si/SiO_x interface.
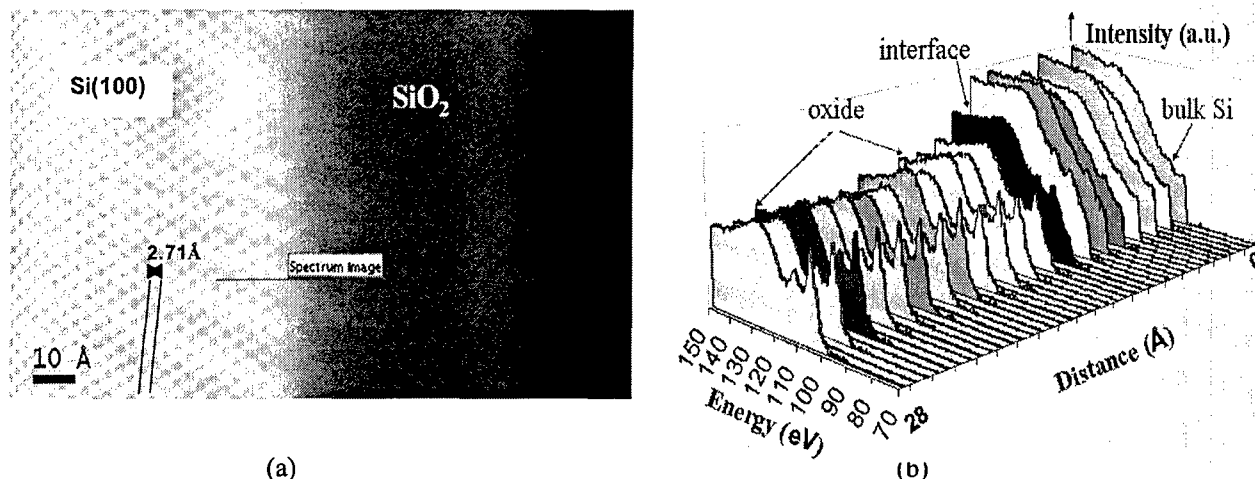

(a)   (b)

Figure 7. (a)High angle annular dark-field (HAADF) image and (b) SiL_{23} edge recorded on the Si(100) oxidized by AO revealing a chemically abrupt interface. An aberration-corrected STEM with image resolution and probe size of 1Å was used.

Hence, we further propose that AO can be directly inserted into the back-bonds, leading to the observed abrupt interface. The initial steps for the Si(100) oxidation by MO are given on the left-hand side of Figure 8, as originally proposed by Watanabe et al. [7].
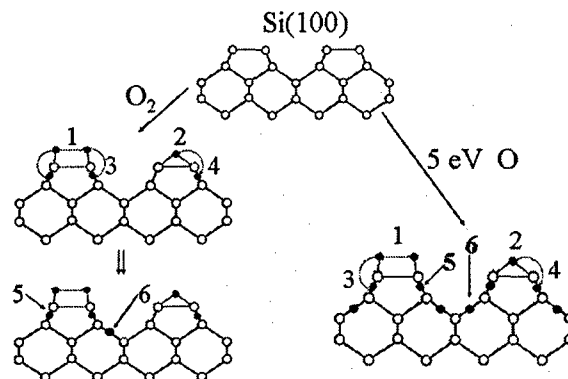

Figure 8. Comparison of the initial steps of Si(100) surface oxidized by atomic oxygen and molecular oxygen.

The first layer backbonds are available via O migration through the metastable surface state that provides the energy (2.96 eV for the top site, position 1, or 5.99 eV for the bridge site, position 2) for the O atom to insert itself into the Si backbonds (positions 3, 4, 5, or 6) while direct O insertion into first or second layer backbond positions 5 or 6 requires energies of 1.0 or 2.4 eV, respectively. The possible steps for the Si(100) oxidation by AO are represented on the right-

8

hand side in Figure 8. The AO has 5.1 eV energy (with no bonds that need to be broken), so it can directly attack backbonds in the first and even second subsurface layer of Si. Three monolayers can thus be oxidized by AO in the initial step, instead of only one by MO. Hence, the initial rate of oxidation would be increased, resulting in abrupt interface, with less transitional states for AO as compared to MO.

Selected area electron diffraction (SAED) techniques provided structural information about the oxide layer. Selected area electron diffraction revealed that the silica formed by AO on Si(100) is more ordered than the oxide created by MO. Shaper and more pronounced diffraction rings are present in the diffraction patterns of Si(100) oxidized by AO as compared to the diffused haloes characteristic for amorphous structure observed for MO oxidized sample (Figure 9).
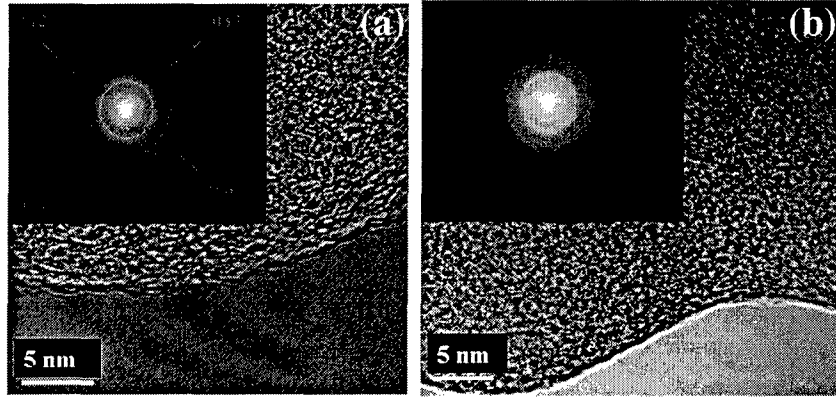

Figure 9.   Plan-view TEM micrographs and SAED patterns of Si(100) oxidized (a) by hyperthermal atomic oxygen (b) by molecular oxygen.

The experimental lattice spacings obtained from the SAED for the oxide created by reactive AO species correspond to that of alpha-quartz with lattice parameter a = 4.78 ± 0.1 Å, c = 5.13 ± 0.1 Å, where in bulk alpha-quartz [6], a = 4.9134 Å, c = 5.4052 Å. The smaller lattice parameters of the oxide formed by AO as compared to bulk alpha-quartz suggest that this oxide is under compression.

Fluctuation electron microscopy (FEM) utilizes hollow cone annular dark field imaging as a function of the k-vector (reciprocal space) utilized to form the dark field image. Fluctuation electron microscopy studies were performed by Prof. Paul Voyles group (Univ. of Wisconsin-Madison) where the variance, V, of the diffracted intensity from nanometer-sized volumes. V is given by the following equation:

$$V(k,Q) = \frac{\langle I^2(r,k,Q) \rangle}{\langle I(r,k,Q) \rangle^2} - 1$$

where
I(r,k,Q) = the measure of the diffracted intensity as a function of position,
K = diffraction vector
Q = radius of the aperture in diffraction space (1/Q is proportional to spatial resolution).

This variance is sensitive to the correlation between 3 and 4 atoms that provides statistical information of the medium range order, i.e. on the length scale of 10-20Å. Variance curves of the Si oxidized by AO and MO are shown below (Figure 10). Each curve is the average of 10 data curves and the scale bars are the standard deviation of the mean. Clearly, the MO

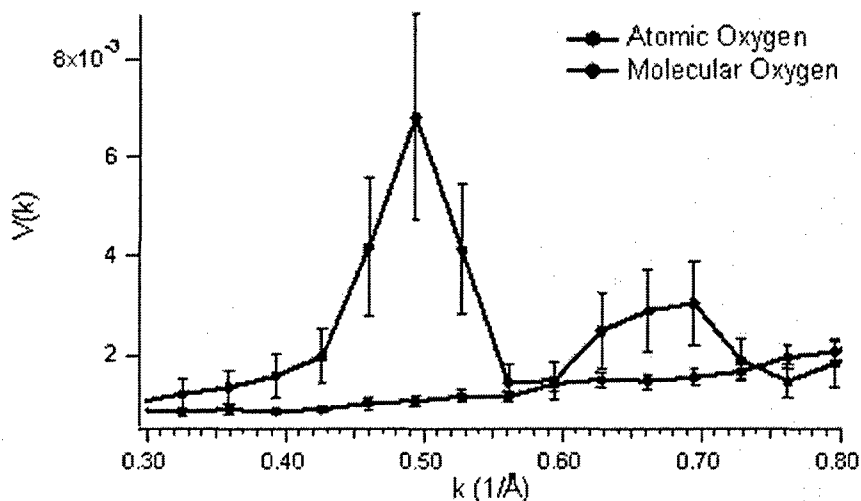formed oxide shows a random arrangement of atoms, whereas the AO formed oxide reveals more medium range order.

Figure 10. V(k) of the oxides formed by exposure of Si to atomic oxygen (black) and molecular oxygen (blue).

The Radial Distribution Functions (RDF) of these oxides will be determined in order to obtain interatomic distances and bond angles. This method will help to identify /confirm crystalline form of silica structure (alpha-quartz) that is formed by AO oxidation. Further modeling of the amorphous structure of the silica with FEM results will provide information about the identity and sizes of the nanocrystallites, as well as their density and possible porosity.

The Effects of Au Overlayer on Si: As an extension of the Si oxidation work, we examined how Au overlayers on Si could protect it from oxidation attack using primarily synchrotron X-ray diffraction. Our initial work was based at NSLS Brookhaven, where we operate an in-situ UHV diffractometer, which is ideally suited to the study. We then switched to the newer Advanced Photon Source at Argonne, which has much brighter beams and allows us to exploit the coherence for certain kinds of problems. Since access to ion beam and plasma sources of energetic oxygen were available at the synchrotron site, we used this as the reactive oxygen source. We investigated the effects of thin (submonolayer) coatings of gold on known Si surface structures, which might induce a certain amount of resistance to oxidation effects. We discovered that the passivation of the Si(111) surface with low coverage Au renders the Si surface partially stable. We have tried to passivate the Au/Si surface using Hydrogen derived from methanol vapor as a passivation agent. Exposing this double passivated surface to atmospheric air was found to keep the structure ordered up to 20% (estimated by diffraction intensity) as compared to complete destruction following only Au passivation. This dual passivated surface now could be a better surface to serve as an oxidation resistant surface.

C.1.b.iii. Nanocrystalline GeO₂ Formed on Ge(100) by Hyperthermal AO

The oxidation of Ge(100) in AO as compared to O_2 showed quite similar phenomena as Si(100). The oxide thickness increased, the interface was chemically abrupt and the oxide was noted to be homogeneous with a structure similar to quartz. Germanium(100) crystals were exposed to 5eV atomic oxygen at 25°C and 200°C gave similar oxide thicknesses of 2-3 nm demonstrating that the energy of the AO species, rather than temperature plays the key role in the amount of Ge consumed during AO exposure. In comparison to Ge(100) exposed to O_2 at 200C, <1nm oxide formed (figure 11). For increasing eV, the oxide thickness increased from 2.5, 4 to 5nm as the kinetic energy of the AO increased from 5, 9, to 15 eV, respectively.
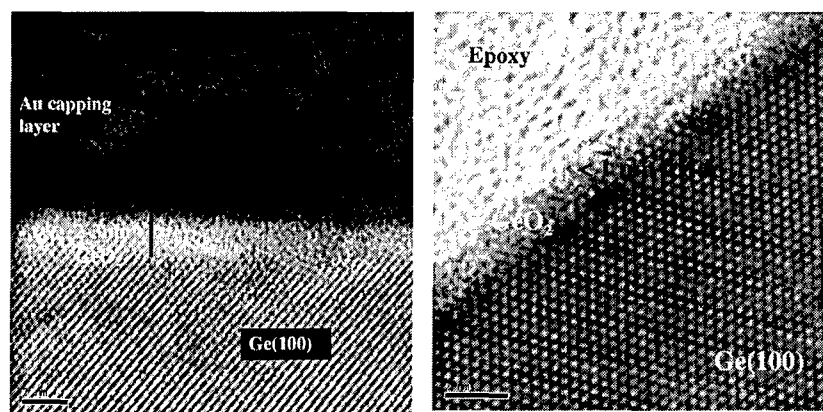

Figure 11. Cross-sectional HRTEM micrographs of the Ge oxide layer formed on Ge(100) oxidized by a) AO b) O_2 at 200°C
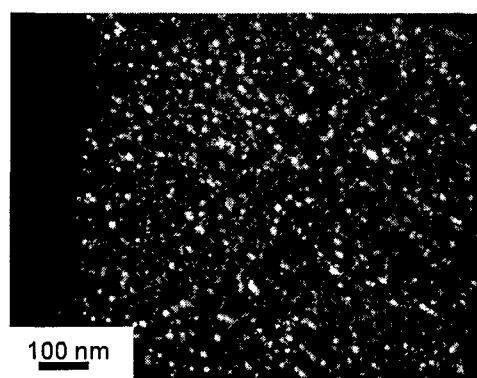

Figure 12. Dark-field image of GeO₂ revealing 1-10nm nanograins after Ge(100) is oxidized in 5eV AO.

Unlike Si oxidation, the oxide formed on Ge was not amorphous, but consisted of crystalline nanograins of GeO_2. Oxidation in O_2 at 200°C gave larger grain sizes of 20-70 nm, whereas oxidation in 5, 9 or 15eV AO at 200°C all gave 1-10nm GeO_2 nanograins (figure 12).

To gain insights into the oxidation kinetics of Si and Ge, QCM experiments were performed *in situ* on polycrystalline Si and Ge films with hyperthermal AO at room temperature. Deviations from the parabolic growth were noted for polycrystalline Si and Ge oxidized in both 5 eV and 9eV AO. Changes in the oxide structure during oxidation could explain the deviations from parabolic kinetics, since the diffusion of the O atom would change with respect to time if the oxide structure changes with respect to oxidation time.

11

C.1.c. Effects of Hyperthermal Atomic Oxygen on Metals

C.1.c.i. The Initial Vaporization of Al Followed by Oxide Growth

Aluminum, similar to Si, forms a very thin (~3nm) amorphous oxide when exposed to oxygen at ambient temperatures. Aluminum and its alloys are used as structural components on space vehicles, and as a coating material to enhance reflectivity and also as protective coating for polymers since the passivation of aluminum after exposing to oxygen. Our initial characterization studies indicated that Al, like Si, forms a thicker and more ordered oxide when exposed to hyperthermal AO. Due to experimental challenges of cleaning Al films *ex situ*, separating the effects between air and AO exposure was difficult. However, interesting results were obtained on the structure and, especially, the kinetics of Al oxidation by AO that were supported by theoretical simulations.

Single crystal Al(100) oxidized by atomic oxygen and the oxide formed by electrochemical oxidation was compared by grazing incidence X-ray diffraction. An additional peak was observed in the AO-oxidized Al, indicating a different and possibly more ordered structure of the alumina (Figure 13).
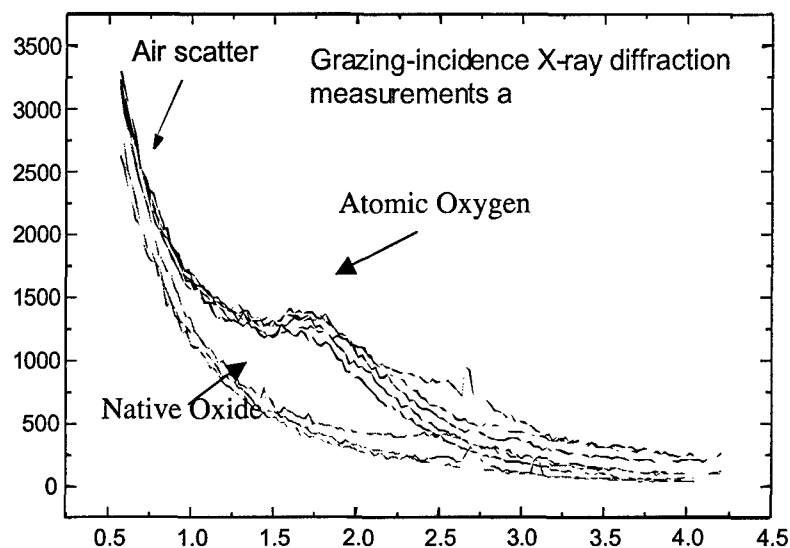

Figure 13: Grazing incidence XRD measurements of Al(100) oxidized in AO (black line) and electrochemical passivation (red line).

We have also characterized the resulting oxide and interface structures by cross-sectional (scanning) transmission electron microscopy ((S)TEM) and scanning electron microscope(SEM) (figure 14). Our TEM results show that an amorphous aluminum oxide layer with ~6 nm thickness formed on the aluminum crystal, and a rough alumina/Al(100) interface forms. From *in situ* QCM studies in the UPitt's FAST AO source, the Al film initially experiences an intriguing mass loss, and then parabolic mass gain (figure 15). To observe the structural evolution of the oxide, a very thin Al (100) single crystal was exposed inside the AO source, characterized by SEM and TEM. The surface morphology changed from flat to rough after 5.5 minutes of exposure. This surface roughening could be related to the initial mass loss measured by QCM.

To understand the mechanism of this initial mass loss, we used a combination of electronic structure theory and classical molecular dynamics calculations to do direct simulations of the collision process. These calculations are technically challenging, so important issues that we had to deal with were what level of electronic structure theory to use, and what structure

12

model of the surface we should use. To assess these questions, we spent significant time examining the use of density functional theory and semiempirical theory, and we studied the interactions of atomic oxygen with aluminum clusters and with slab models of aluminum surfaces. A serious problem in this work was incorrect conversion of triplet atomic oxygen plus a singlet aluminum cluster to a singlet atomic oxygen plus a triplet cluster. While this might correctly occur at short range between the atom and surface, we found that it was an important, but spurious, process even at long range, particularly for larger clusters and for slab models of the surface. The problem could be fixed "by hand" by forcing the orbital occupations, but this was not feasible for trajectory studies. To circumvent this, we chose to work with small Al clusters (up to Al_{13}).
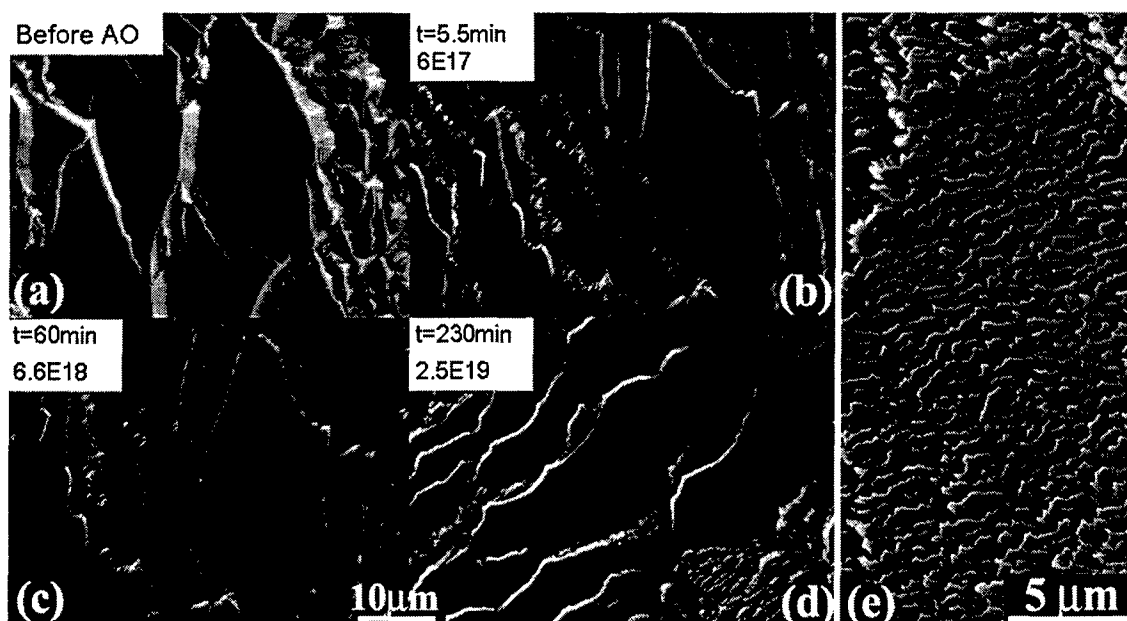

Figure 14. Series SEM images of the evolution of oxide on Al(100), showing a rough surface after exposing to AO.
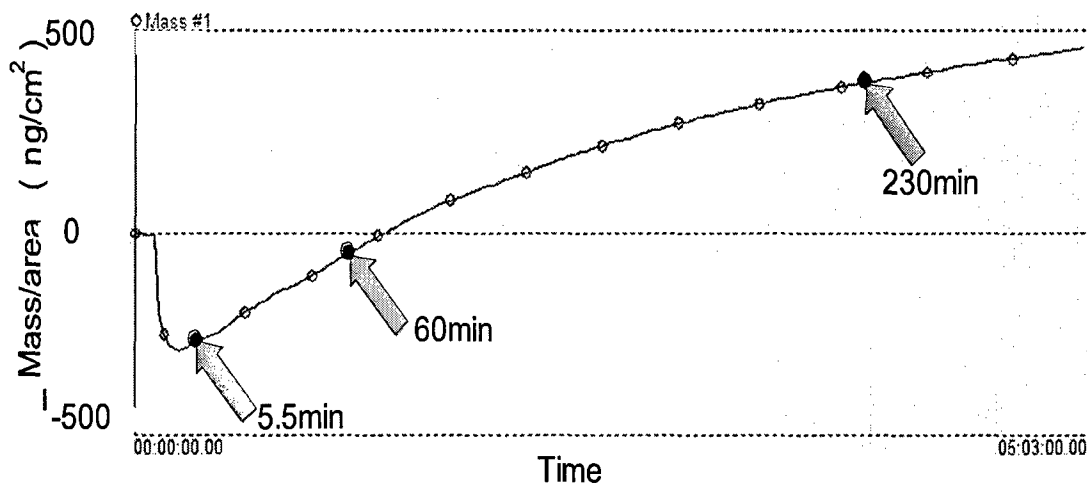

Figure 15. Dynamical mass loss prior to mass gain when Al is exposed to 5eV AO.

Figure 16 shows a typical energy level diagram that we have produced using density functional theory (B3LYP), in this case for O + Al$_3$. This shows that reaction involves the formation of an Al$_3$O intermediate, as expected. This intermediately dissociates to Al$_2$O + Al, which is a particularly stable product. Other possible species such as AlO can also occur but this is a relatively minor product. The reason for this is that the Al$_2$O is a strongly ionic species that can be thought of as (Al^{1+})$_2$(O^{2-}), while AlO is less ionic (roughly Al^{1+}O^{1-}). Higher clusters of the form Al$_n$O can be thought of as the ionic Al$_2$O in combination with neutral additional neutral atoms, and thus have weaker differential stability. We have simulated atomic oxygen collisions with several small clusters, and we find that Al$_2$O is always the dominant oxygen containing product. This suggests that the mass loss involves Al$_2$O formation at the surface, followed by its ejection into the gas phase.
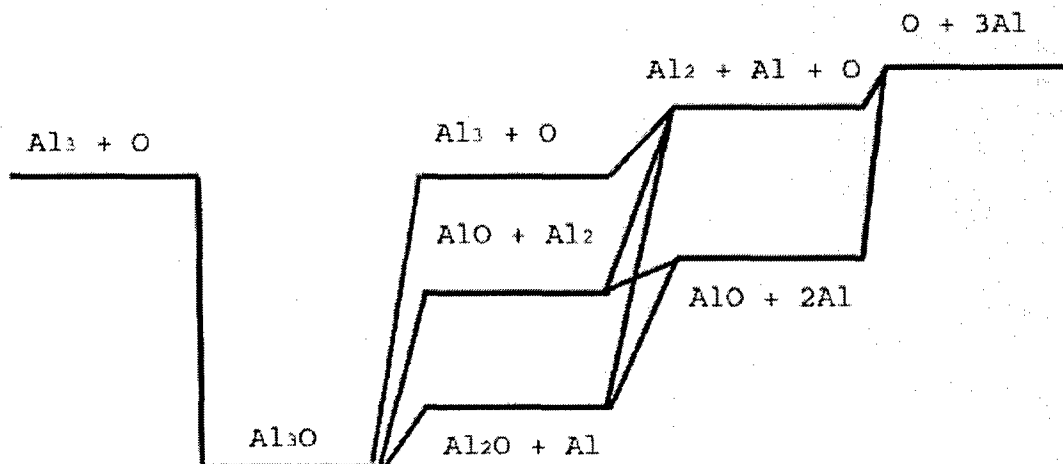

Figure 16. Energy levels from B3LYP/DZVP calculations for O + Al$_3$. The energy units are such that the Al$_3$O minimum is 8.41 eV below O + Al$_3$

C.1.c.ii. Ag Oxidation by Atomic Oxygen:

Bulk single crystals of Ag (100) and Ag (111) were exposed simultaneously under same conditions at 220°C by atomic oxygen with the flux of 3×10^{15} atoms.cm^{-2}s^{-1} for 7 hours, where the 5.1eV atomic oxygen are created by laser detonation of oxygen gas. X-ray diffraction of Ag oxide layer, revealed that Ag$_2$O is the main product of silver reacted with atomic oxygen. The existence of additional Ag XRD peaks, besides the {100} family of planes for Ag(100) and the {111} family of planes for Ag(111), demonstrate that polycrystalline silver exists in both orientations of oxidized Ag. Furthermore, XRD reveals different oxide compounds for the two different orientations of Ag. The products of Ag (100) oxide layer are polycrystalline Ag, Ag$_2$O, and, notably, Ag$_2$O$_3$. The products of Ag (111) oxide layer are polycrystalline Ag, Ag$_2$O, and, notably, Ag$_3$O$_4$.

The bright field TEM images of the cross-section of the Ag (100) oxide layer revealed a broad intact interface between the Ag single crystal and the oxide layer, where an intermix zone between the oxide and metal exists. The oxide layer consisted of a complex microstructures, such as porosity, micro-twins and irregular shaped grains. The electron diffraction pattern from the silver crystal to the oxide scale showed the presence of polycrystalline silver. Energy dispersive

X-ray spectroscopy confirmed the "oxide scale" to contain *mostly* Ag (the oxygen detected was 3-5 at. %) (figure 17). The oxidation by hyperthermal atomic oxygen produces polycrystalline structures of mostly Ag and small amount of different Ag oxide compounds.
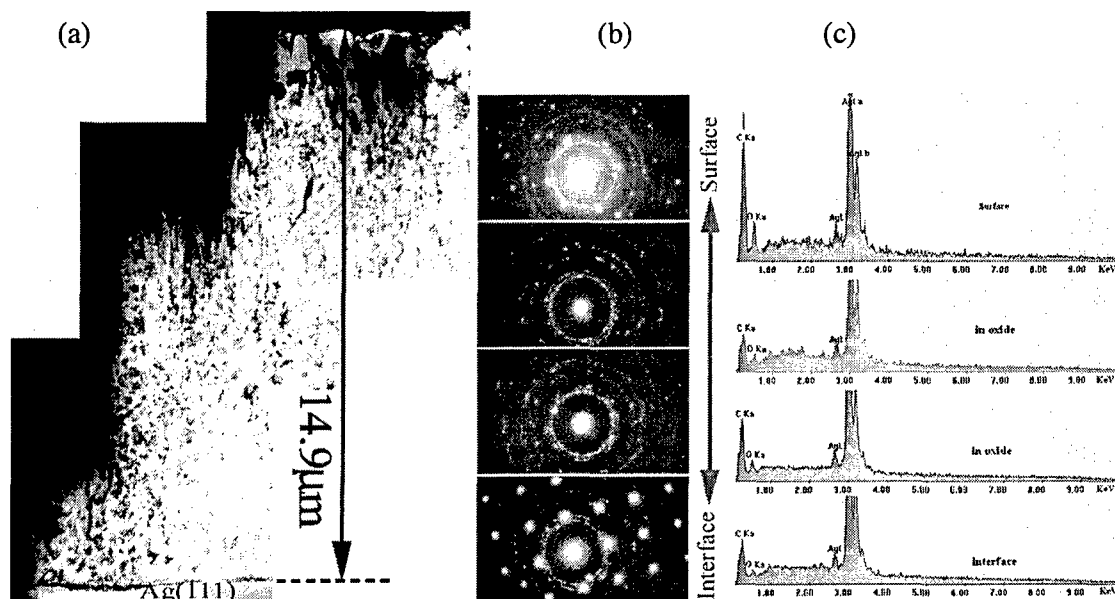

Figure 17: (a) Cross-sectional TEM image of Ag(111) oxidized by 5eV atomic oxygen. (B) Selected area electron diffraction pattern indicating polycrystalline Ag. (c) EDS plots corresponding to the same region shown in (b), where 3-5% O detected.

C.1.d. Additonal Secondary Effects in LEO

C.1.d.i. Electrostatic Field Enhancement of Al Oxidation and Limited Memory Effects on Si Oxidation

We have observed that the electrostatic charging of an aluminum oxide film by electron bombardment produces a greatly enhanced rate of Al(111) oxidation by O_2(g) at 90 K, compared to a film which has not been bombarded by electrons. The negative electrostatic charge, deposited in the process of electron irradiation of the outer surface of the film, causes rapid oxide film growth, when molecular O_2 is incident on this charged surface. An enhancement of the oxidation rate occurs during electron bombardment, but, surprisingly, also *after bombardment is discontinued*. This "memory effect" for prior electron bombardment shows that this phenomenon is not due to electron stimulated excitation of adsorbed O_2 species on the surface, but instead to an electric field effect within the oxide film.

Figure 18a shows the oxide film thickness as a function of oxygen exposure after the various electron-assisted oxidation procedures, interrupted for XPS film thickness measurements. At the end of the initial electron-assisted oxidation period (point A) (after the 2100 L O_2 exposure, 1 L = 1 x 10^{-6} Torr x s), the extent of oxidation had reached a near-saturation condition. The oxygen gas was then evacuated, and electron bombardment was carried out in ultrahigh vacuum at 100 eV, depositing 1.5 x 10^{-3} C/cm^2 of charge at a current density of 5 μA/cm^2. At this point, irradiation by electrons was discontinued, and the surface was then periodically exposed to O_2(g) at 1x10^{-7} Torr as sequential XPS measurements were made. It was observed that extensive

additional oxide film growth occurs on the charged surface after the termination of the electron bombardment. In contrast, if no charging by electron irradiation was carried out, the oxide thickness remained essentially constant upon exposure to O_2 as shown by the horizontal line in Figure 18a (circles) beyond point A. These data were obtained in a separate experiment and plotted after normalizing the oxygen coverage at point A. The electron irradiation dose at point A was carried out to different levels, and it was found that after a charge of 1.5×10^{-3} C/cm^2 was applied, independently of the electron beam current density or electron dose duration, no further enhancement of the oxidation rate was observed, indicating saturation of the stored surface charge density.

The rate of field-induced oxidation is linearly correlated with the degree of surface charging. The charging of the oxide layer observed here is a result of the capacitor-like behavior of the Al_2O_3 insulator film. The grounded Al metal is one of the plates of the capacitor, and the negatively charged outer part of the oxide layer is the other. At 90 K under the O_2 exposure conditions used here, substantial quantities of adsorbed molecular oxygen may be stored on the oxide surface. Electron tunneling from the metal to the surface of the oxide film can lead to conversion of adsorbed O_2 into O_2^- ions, leading to the dissociation and formation of O^{2-} ions. The high electric field induced by the surface charging will enhance the mobility of Al^{3+} and O^{2-} ions through the oxide film, promoting the oxide film growth.

According to the accepted Cabrera-Mott theory of low temperature metal oxidation, an electrostatic field formed across a growing oxide film promotes ion diffusion - the rate limiting step for mass transport in oxidation. In thermally activated metal oxidation, electron tunneling from the bulk metal to the affinity level of the oxidizing species occurs, and the electric field produced across the oxide film thickness controls the rate of ion transport and concomitant oxide film growth. However, in the case of thermal oxidation, the value of the electrostatic potential on the outer part of the oxide film gradually decreases as $1/d$ (where d is the thickness of the growing oxide film), as the electron tunneling through the growing layer diminishes, leading to the parabolic oxide growth rate observed. Creation of the electrostatic potential by means of electron irradiation allows for the artificial stimulation of the ion diffusion, and film growth after the apparent saturation of the thermal growth was achieved.

In these experiments, the artificial production of enhanced negative charge on the surface of a stable oxide film has been shown to induce additional metal oxidation when oxygen is subsequently added to the charged surface. This phenomena impacts material utilized in the space environment where many charged species and plasmas exist.

Because of the previous demonstration that electric fields of the order of 10^7 V cm^{-1} produce an enhancement in the rate of oxidation of Al(111) by O_2, similar experiments were performed on Si(100) to search for a similar effect (figure 18b). Using electron bombardment to cause surface charging, the oxidation kinetics for Si(100) were investigated before and after charging by electron bombardment. No effect was found for Si(100). This may be understood by the fact that the formation of SiO_2 involves primarily the formation of covalent bonds, where, in contrast to Al_2O_3 thin film formation, ion migration is not involved in controlling the kinetics of oxidation and electric fields would be expected to have little effect. The good news from this work is that silicon surfaces in orbit would not be expected to be oxidized by negative surface charge buildup from the negative plasma. A paper on this has been submitted to *The Journal of Vacuum Science and Technology A*. Figure 18 illustrates the comparison of the charging effect on Al and Si.
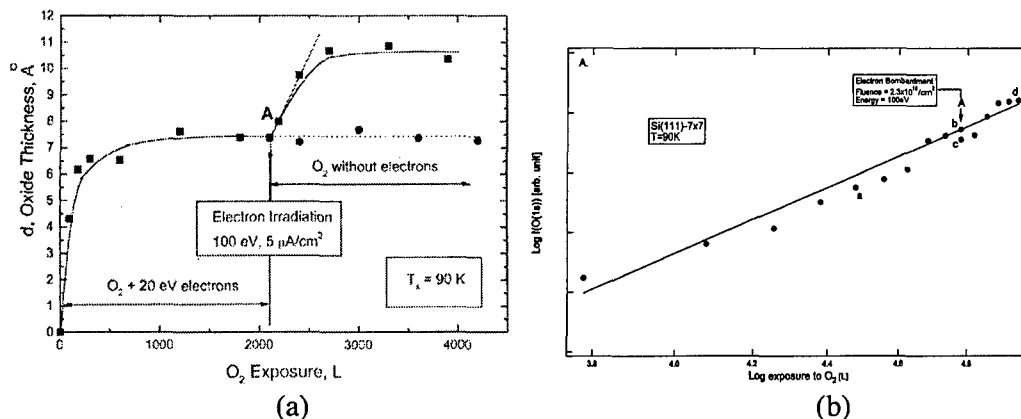
16

Figure 18. (a) The the dramatic effect on Al of electron charging during oxidation and (b) limited effect on Si.

D. IMPACT TO AIR FORCE AND DOD OBJECTIVES

One immediate and practical impact to the Air Force (and DoD) of determining the dramatically different fundamental oxidation mechanisms of hyperthermal atomic oxygen on metals, and semiconductors is that these materials and are used as coating materials on polymer materials for protection and dissipation of static charge. Silver is of interest because it is used to monitor AO fluence as well as line microwave cavities. The metal or semi-conductor material will passivate due to exposure to AO and form a protective oxide protecting the underlying polymer material. The consequence of these structural studies and new models of AO oxidation is to lead to smarter coating designs.

E. PUBLICATIONS:

[1] I. Popova, V. Zhukov, J. T. Yates, Jr., "Electrostatic Field Enhancement of Al(111) Oxidation", Phys. Rev. Let., 89, p. 276101 (Dec. 2002).

[2] I. Popova, R. Muha, Z. Chen and J. T. Yates, Jr., "Construction and performance of a low energy ion gun", J. Vac. Sci. Tech. A, 21, p. 401 (2003).

[3] S.-Y Ohno and J. T. Yates, Jr., "Electron Impact Effects on the Oxidation of Si(111) at 90K", Journal of Vacuum Science and Technology 23(3) p. 475 (2005).

[4] S.K. Ghose, I. K. Robinson and R. S. Averback, "Defect formation in Si(111)7x7 surfaces due to 200eV Ar+ ion bombardment", Phys. Rev. B, 68 165342 (2003).

[5] S. K. Ghose, P. A. Bennett and I. K. Robinson, "Nanoclustering of Au on the Faulted Half of the Si(111)7x7 Unit Cell", Physical Review B, 71 073407 (2005)

[6] S. K. Ghose, P. A. Bennett, I. K. Robinson and F. J. Himpsel, "Structure of Double-Row Quantum Wires in Au/Si(553)" , Surface Science 581 199-206 (2005)

[7] Y. Zhong, C. Bailat, R. S. Averback, S. K. Ghose and I. K. Robinson, "Damage

17

accumulation in Si during high-dose self-ion implantation" <u>Journal of Applied Physics</u> 96 1328-1335 (2004)

[8] M. Kisa, T. Minton, and J.C. Yang,,"Structural Comparisons of SiOx and Si/SiOx Formed by the Exposure of Silicon (100) to Molecular Oxygen and to Hyperthermal Atomic Oxygen", <u>J. Applied Physics</u> (2004)
[9] M. Randjelovic, J. C. Yang. "Structural comparisons of passivated Si(100) by atomic and molecular oxygen" <u>Materials at High Temperatures</u> (2003), 20(3), 281-285.

[10] M. Kisa, L. Li, J. Yang, T. Minton, W. Stratton, P. Voyles, X. Chen, K. van Benthem and S. Pennycook "Homogeneous Silica Formed by the Oxidation of Si(100) in Hyperthermal Atomic Oxygen" <u>Journal of Spacecrafts and Rockets</u> 43 (2), 431 (2006)

[11]. J. Middendorf, C. Aikens and G. C. Schatz, "Theoretical studies of the reaction of atomic oxygen with aluminum clusters", J. Phys. Chem., to be published.

[12]. R. Harder, L. Li, J. C. Yang and I. K. Robinson, "Crystallinity changes in Indium-Tin Oxide thin films due toexposure to Atomic Oxygen", in preparation for Journal of Vacuum Science and Technology (2006)

[13]. L. Li, T. Minton and J. Yang. "Unusual oxidation-reduction of Ag(100) to polycrystalline Ag by hyperthermal atomic oxygen", in preparation for J. Phys. Chem. B (2006).

[14]. M. Kisa, R. Harder, I,K. Robinson and J. C. Yang, "Structural oxide changes due to exposure of Ge to hyperthermal atomic oxygen", in preparation for J. Applied Physics (2006).

[15]. M. Kisa, L. Li and J.C. Yang, "Oxidation kinetics of Si and Ge exposed to hyperhermal atomic oxygen", in preparation for Physical Review Letters (2006).

[16]. L. Li, T. Minton, J. Middendorf, C. Aikens , G. C. Schatz, and J. Yang. "Atypical vaporization of Al during the initial oxidation stages of Al in hyperthermal atomic oxygen", in preparation for J. Phys. Chem. B (2006).

Conference Proceedings

[1]. Long Li, Ross Harder, Fengting Xu, Ian K. Robinson and Judith C. Yang, "Characterization of Structural Change of Nano-crystalline ITO Films due to Exposure to Hyperthermal Atomic Oxygen", *Microscopy and Microanalysis,* 321, Volume 12, Supplement S2 (2006)

[2]. Long Li, Ross Harder, Fengting Xu, Ian K. Robinson and Judith C. Yang, "Degradation of Nano-crystalline ITO Films due to Exposure to Hyperthermal Atomic Oxygen", *Mat. Res. Soc. Symp. Proc.,* 0887-Q10-08, V887 (2006).

[3]. Long Li, Timothy K. Minton and Judith C. Yang, "Structural Characterization of Aluminum Oxidation due to Exposure to Hyperthermal Atomic Oxygen", *Microscopy and Microanalysis,* 1986-1987, Volume 11, Supplement 2 (2005).

[4]. Long Li, Liang Wang, Timothy K. Minton and Judith C. Yang, "Structural Characterization of Oxide Layers on Aluminum Formed by Exposure to Hyperthermal Atomic Oxygen", *Mat. Res. Soc. Symp. Proc.* NN9.4, V851 (2005).

18

[5]. Judith C. Yang, Huiping Xu, Long Li, Deborah Waters, and Bruce Banks, "TEM Studies of Protective Al Coatings on Kapton H" *Mat. Res. Soc. Symp. Proc.* NN9.8, V851 (2005).

[6]. Maja Kisa, William G. Stratton, Timothy K. Minton, Klaus van Benthem, Steve J. Pennycook, Paul M. Voyles, Xidong Chen, Long Li, and Judith C. Yang, "Increased Ordering in the Amorphous SiOx due to Hyperthermal Atomic Oxygen", *Mat. Res. Soc. Symp. Proc.* NN9.5, V851 (2005).

[7]. Long Li and Judith C. Yang, "Structural Changes of Ag Single Crystals by Exposure to Hyper-thermal Atomic Oxygen" *Microscopy and Microanalysis,* 286, Volume 10, Supplement 2 (2004).

[8]. Long Li and Judith C. Yang, "Formation of Nanosized Metallic Ag Grains by Oxidation of Ag Single Crystals with Hyperthermal Atomic Oxygen", *Mat. Res. Soc. Symp. Proc.* L1.3, V788 (2004).

[9]. Long Li and Judith C. Yang, "Structural Characterization of Broad Oxide Layers of Ag Single Crystals Caused by Hyperthermal Atomic Oxygen by SEM and TEM", *Microscopy and Microanalysis,* 686, Volume 9, Supplement 2 (2003).

[10]. Long Li and Judith C. Yang, "Oxide Structures formed on Silver Single Crystals due to Hyperthermal Atomic Oxygen Exposure", *Mat. Res. Soc. Symp. Proc.,* Z3.37.1, V751(2003).

[11]. Maja Kisa, Ray D. Twesten, and Judith C. Yang, "Structural Comparisons of SiOx and Si/SiOx Formed by Passivation of Single-Crystal Silicon by Atomic and Molecular Oxygen" *MRS Proceedings* Vol *786 (2003)*

[12]. Maja Randjelovic; Judith C. Yang "A structural comparison of Si(100) oxidized by atomic and molecular oxygen" *Materials Research Society Symposium Proceedings (2001),* 751, 127-132.

F. MAJOR ACCOMPLISHMENTS:

1. The primary accomplishment of this MURI team was demonstrating that completely different oxides form due to exposure to hyperthermal atomic oxygen, and, hence, novel oxidation mechanisms are needed to explain such unusual oxide structures.

    ITO: the reactivity of AO causes recrystallization of the ITO nanograins along the interface between the ITO and substrate, which would negatively affect the film adhesion.

    Si: Remarkably homogeneous and uniform oxides form that are thicker and more ordered towards the alpha quartz structure than the oxide formed by O_2 exposure, due to the high reactivity of the AO and its kinetic energy.

    Ge: The effect of the AO is to produce smaller nanograins of crystalline GeO_2 as compared to O_2, where increasing the kinetic energy increases the oxide thickness.

    Al: The AO causes initial vaporization and corresponding roughening of the Al surface prior to the growth of the amorphous oxide scale, which could be due to the formation of gaseous and stable AlO_2.

    Ag: The unexpected effect of AO on Ag is not to primarily oxidize the Ag to a Ag oxide species, but to transform the single crystal Ag to polycrystalline Ag possibly due to a simultaneous oxidation and reduction of the Ag.

2. The development of a unique UHV hyperthermal atomic oxygen source with heating and VUV exposure capabilities to best mimic the environment in LEO. Additional QCM permits *in situ* studies of the oxidation kinetics and the portability of this instrument allows the interfacing of this unique source to other advanced instruments, that are note moveable, at different research sites.

3. Dramatic memory charging effect by electrons for the oxidation of Al, in contrast to the limited effect of charging on Si oxidation.

G. HONORS

John T. Yates, Jr. is a R. K. Mellon Professor of Chemistry, University of Pittsburgh since 1981. He is a Member of the National Academy of Sciences (1996), and the recipient of the von Humboldt Senior Scholar (1995-1997) and the J. Linnett Professorship from Cambridge University (2000).

Ian Robinson (Physics, University of Illinois at Urbana-Champaign) is a Fellow of the American Physical Society and the 2000 winner of the B. E. Warren Diffraction Physics Award of the American Crystallographic Association.

Robert Averback (Materials Science and Engineering, University of Illinois at Urbana-Champaign) is a recipient of the Alexander Von Humboldt, Senior Research Award (1993). He was a co-recipient of the Department of Energy Award for Outstanding Sustained Research in Metals and Ceramics, (1984) and has been recently named as an American Vacuum Society Distinguished Lecturer (1998).

Paul Voyles (Materials Science and Engineering, University of Wisconsin at Madison) is the 2004 recipient of a NSF Career award. He was on the incomplete List of Teachers Ranked Excellent, University of Illinois 1997 and the recipient of the Howe Prize in Physics, Oberlin College 1996.

George Schatz (Chemistry, Northwestern University) is an elected member of the International Academy of Quantum Molecular Sciences and the American Academy of Arts and Sciences. He is a fellow of the American Physical society and recipient of the Alfred P. Sloan Research Fellow Camille and Henry Dreyfus Teacher-Scholar Fresenius Award Fellow.

Judith C. Yang (Materials Science and Engineering, University of Pittsburgh) is the 2002 recipient of a NSF Career Award on fundamental oxidation investigations and 2003 NASA Faculty Fellowship. She is the recipient of B.P. America Faculty fellowship in 2004, and the 2005 Chancellor's Distinguished Research Award for Junior Faculty.